Biosensors and Bioelectronics 201 (2022) 113972

Contents lists available at ScienceDirect

Biosensors and Bioelectronics

journal homepage: www.elsevier.com/locate/bios

Multifunctional amino acids empowering bifunctional biosensing platform for depression study

Shengnan Yang, Wei Feng, Lan Xue, Mengai Yin, Binshuai Li, Lina Lu, Fuju Dai, Jun Jiao **, Qiang Chen *

The Key Laboratory of Bioactive Materials Ministry of Education, College of Life Science, Nankai University, Weijin Road No.94, Tianjin, 300071, PR China

A R T I C L E I N F O

Keywords:
Depression
Glucocorticoid receptor alpha (GRα)
Electrochemical biosensor
Amino acids
Quantitative analysis

A B S T R A C T

Poor availability of objective approaches hinders effective diagnosis and treatment for depression. Biosensors provide a promising platform for the development of quantitative and practical methods for disease detection, as well as for drug discovery. Here, we developed an electrochemical biosensor has been established with the ability to simply and accurately detect the trace glucocorticoid receptor alpha (GRα), as a key biomarker of depression, in both hippocampus and blood cells. The integration of amino-ion graphene oxide (IL-rGO) and amino acid-coated gold nanoparticles (AA-AuNPs) via green synthesis remarkably magnifies the electrochemical signals, where amino acids play multiple roles as reducing agents, stabilizers, and bridging agents. After the optimization among AA-AuNPs@IL-rGO nanocomposites based on five typical amino acids, a biosensing surface has been constructed to implement analysis in real samples as a bifunctional platform. The obtained biosensor exhibited a remarkably low limit of detection (0.283 pg mL^{-1}) and could thus sensitively identify the GRα differences in healthy and depressive rats with and without fluoxetine. The electrochemical biosensor developed herein was not only outstandingly sensitive but also simple to use and labor-saving, making it a promising all-in-one platform for depression diagnosis and drug discovery.

1. Introduction

Depression is a psychological disease associated with suicidal tendency and aggressiveness, which differs from the feeling of sorrow, stress, or despair (Abbasi and Puusepp-Benazzouz, 2020; Huckins, 2017; Mackin et al., 2021; Rotenstein et al., 2016; Vigo et al., 2016). This disease is projected to become the most widespread disabling condition, affecting more than 300 million people worldwide by 2030 (Gururajan et al., 2019; Malhi and Mann, 2018; Zhou et al., 2021). Currently, the primary means of diagnosis for this disease is through a questionnaire to identify typical signs and symptoms of depression. However, the inherent subjectivity of this approach results in high misdiagnosis rates, leading to delayed diagnosis and a failure to deliver timely treatment (Danczak, 2017; Ferenchick et al., 2019; Gilbert, 2017). Hyperactivity of the hypothalamic-pituitary-adrenal (HPA) axis with glucocorticoid receptor (GR) dysfunction, especially GR alpha (GRα), have been demonstrated to be essential elements in the pathogenesis of major depression (Keller et al., 2017; Milaneschi et al., 2019; Sousa et al., 2020). Further, clinical studies have indicated that GRα is significantly downregulated in severe depression patients compared to their healthy counterparts (Gormley. et al., 1985; Pariante and Lightman, 2008). Variations in the expression of glucocorticoid receptors (GRs) can be utilized to predict unique cognitive functions, among which GRα also is a key indicator to evaluate the performance of different therapies (Canet et al., 2018; D'Alessio et al., 2020; Keller et al., 2017). At present, GRα expression can currently be detected via RT-qPCR, western blotting, and ELISA (Knable et al., 2004; Matsubara et al., 2006; Okada and Okada, 2020; Perlman et al., 2004; Sun et al., 2018). However, each of these methods has its unique disadvantages such as insensitivity and methodological difficulties, and are therefore not well-suited for rapid disease detection in complex biological specimens. In contrast, biosensors offer a quick, simple, and sensitive means to detect trace amounts of a given target in complex samples (Song et al., 2020). Nevertheless, very few biosensors for GRα detection have been thus far developed to meet the growing need for depression diagnosis using biological specimens.

Natural amino acids, the basic building blocks of proteins, are

* Corresponding author.
** Corresponding author.
E-mail addresses: junjiao@nankai.edu.cn (J. Jiao), qiangchen@nankai.edu.cn (Q. Chen).

https://doi.org/10.1016/j.bios.2022.113972
Received 15 September 2021; Received in revised form 18 November 2021; Accepted 4 January 2022
Available online 6 January 2022

environmentally friendly and non-cytotoxic materials and are therefore excellent candidates for the synthesis of biomolecular piezoelectric materials, hydrogels, and chiral nanoparticles (Dou and Feng, 2017; Kim et al., 2020; Lee et al., 2018; Preiss et al., 2015; Xing et al., 2017). Hye-Eun Lee et al. recently have used amino acids to change the handedness, optical activity, and chiral plasmonic resonance of the nanoparticles (Lee et al., 2018). Further, Xing et al. successfully constructed hydrogels based on the complexation of certain aromatic amino acids and bipyridine units (Xing et al., 2017). However, the functions of specific amino acids during the construction process of electrochemical biosensors have remained largely unexplored. Graphene oxide (GO) has recently garnered increasing attention due to its unique physical properties, high volume-to-surface ratio, and excellent electrical conductivity properties (Cai and Yu, 2021; Georgakilas et al., 2016; Lei et al., 2017; Stoller et al., 2008). Mahbubur Rahman et al. developed a sensing platform to detect the circulating tumor DNA using the electrochemical reduction of GO and simultaneous electrodeposition of rGO-AuNSs (Rahman et al., 2020). Additionally, Feng et al. prepared GO via the chemical method and applied it for the detection of hydroquinone and ascorbic acid (Feng et al., 2014). The reduced graphene oxide (rGO) has also been used as a platform for loading AgNPs and carbon nanotubes in order to assemble a bifunctional impedimetric sensors for the quantitative detection of CySH and iodate (Azadbakht et al., 2016). The application of GO, however, is limited by its instability and poor dispersity. Although work is in progress to prevent aggregation, the self-assembly of nanoparticles functionalized by amino acids and functionalized GO has not been fully explored (Matsumoto et al., 2015). Given the high sensitivity of biosensors toward the specific electrochemical properties of the substrate, little is known about the mechanisms by which the combination of functionalized GO and amino acid-reduced nanoparticles enhance biosensor performance.

Here, a simple and environmentally friendly electrochemical biosensor was developed for GRα detection. Based on the specific features of amino acids, gold nanoparticles were greenly synthesized by tryptophan and conjugated with amino-ion graphene oxide to form a hypersensitive sensing platform. To achieve a high sensitivity at trace concentrations, the performances of various amino acid-coated gold nanoparticles were investigated, which was essential to achieve optimal antibody immobilization and antigen capture. Under the optimized conditions, the proposed sensing system could rapidly detect the even slight variations in GRα levels. Additionally, the outstanding properties of the developed sensor make it not only uniquely well-suited for the detection of GRα variations in the hippocampus and blood cells of healthy and depressive rat models but also to assess GRα alterations after

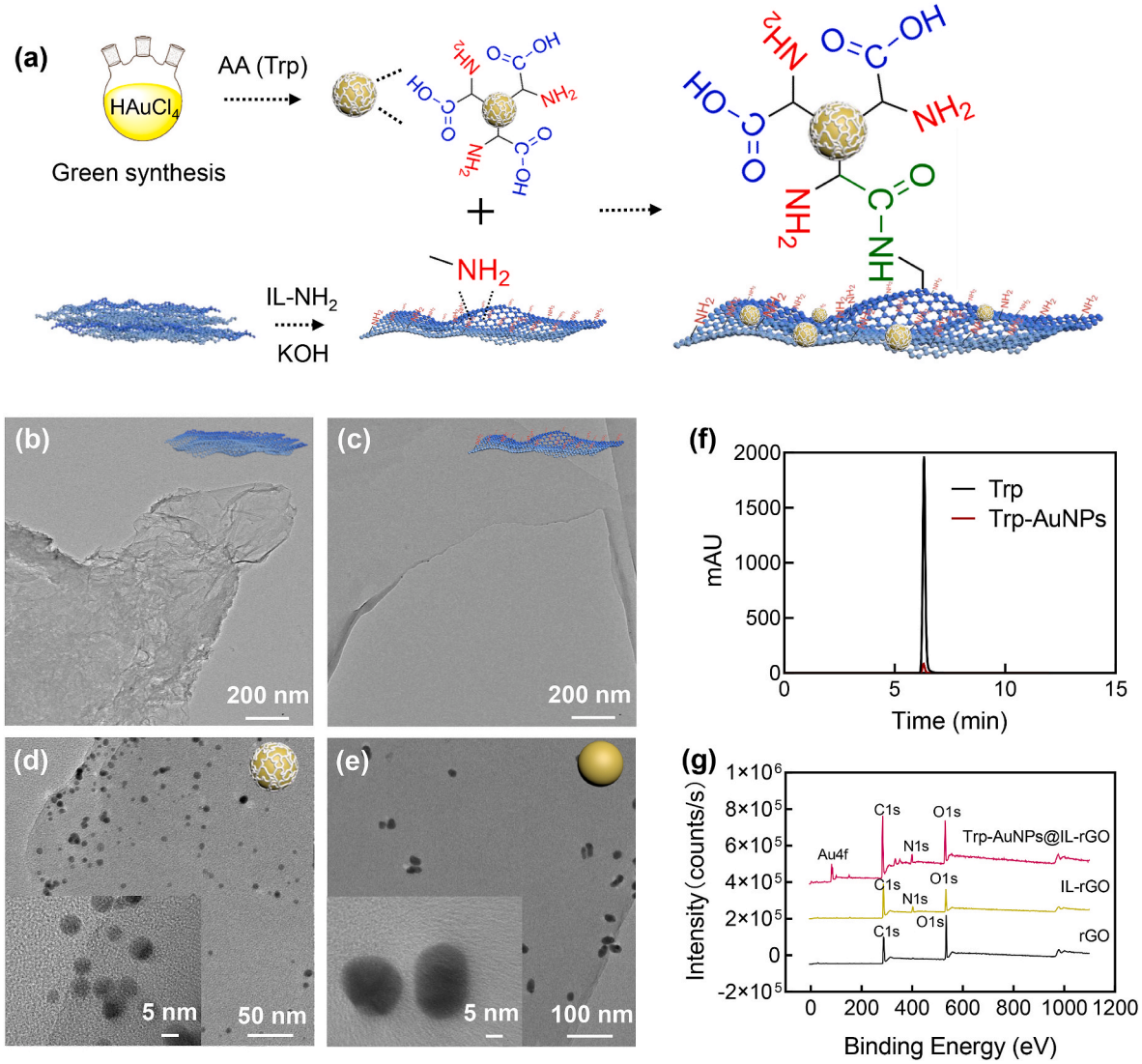

Fig. 1. Synthesis of Trp-AuNPs-IL-rGO (a) and characterizations of rGO, IL-rGO, Trp-AuNPs@IL-rGO, and AuNPs@IL-rGO; (b) TEM image of rGO; (c) TEM image of IL-rGO; (d) TEM image of Trp-AuNPs@IL-rGO; (e) TEM image of AuNPs@IL-rGO; (f) HPLC of Trp-AuNPs and the Trp; (g) survey spectrum of XPS.

treatment with a classic antidepressant drug. This distinguished biosensor thus provides an all-in-one solution for both depression diagnosis and pharmaceutical evaluation of new drugs.

2. Results and discussions

2.1. Characterization of Trp-AuNPs@IL-rGO nanocomposites

To establish a stable sensing surface with high electrochemical activities, IL-rGO nanosheets loaded with Trp-AuNPs were synthesized as the matrix. Fig. 1a shows the synthesis process of AA-AuNPs@IL-rGO with tryptophan (Trp) as an example. The AuNPs were reduced in situ by amino acids (AAs), resulting in a high number of amino(-NH_2) and carboxyl (-COOH) groups on their surface. Further, amine-terminated ionic liquid (IL-NH_2) was introduced into IL-rGO, thereby increasing the number of exposed -NH_2 groups on the surface of rGO. Therefore, the incorporation of AA-AuNPs and IL-rGO via the physical adsorption and through the amide bond condensed between the amino group and the carboxyl group provide optimal conditions for uniform AA-AuNP attachment.

Transmission electron microscope (TEM) was used to inspect the morphology characteristics of the obtained nanomaterials. Compared with pristine rGO, a smoother lamellar structure was observed in the TEM image of IL-rGO after functionalization with IL-NH_2 (Fig. 1b and c), thus providing more binding sites for further modification to enhance sensitivity (Xu et al., 2019). A 24 h stationary experiment also confirmed that IL-rGO had good dispersibility and long-term stability without a tendency to deposit and agglomerate (Fig. S1). Fig. 1d and e compare the TEM images of AuNPs@IL-rGO with the different reductants, namely trisodium citrate and amino acid Trp. As observed in these figures, the nanoparticles were evenly distributed on the IL-rGO nanosheets, indicating that chloroauric acid had been successfully reduced into AuNPs. Rather than the size and distribution of AuNPs reduced by trisodium citrate, the ones reduced by Trp exhibited a more regular round shape (6 nm diameter on average) and were more uniformly attached to IL-rGO. This was likely because the Trp-AuNPs were rich in the carboxyl groups, which can interact with a commensurate amount of amino (-NH_2) groups on the IL-rGO surface to establish a specific and stable connection (Yu et al., 2016). Additionally, the Trp-AuNPs had a shorter synthesis time and exhibited higher yields than its trisodium citrate-generated counterparts, indicating that Trp was not only a good stabilizer but also a favorable reductant for the synthesis of Trp-AuNPs@IL-rGO.

The components of the Trp-AuNPs@IL-rGO nanocomposites were determined via TEM elemental mapping analysis and energy dispersive X-ray (EDX) spectroscopy (Fig. S2). The results showed that the obtained nanohybrids consisted of Au, Cl, O, and N, indicating that Trp-AuNPs@IL-rGO had been successfully prepared. Moreover, high-performance liquid chromatography (HPLC) was conducted to verify the existence of tryptophan through alkaline hydrolysis detected at a 280 nm wavelength. As shown in Fig. 1f, standard tryptophan as the control group displayed an obvious peak at a retention time of 6.215 min, whereas the supernatant after Trp-AuNPs centrifugation also had a similar retention time of 6.214 min, further confirming the successful introduction of Trp.

XPS characterization was employed to analyze the surface chemical composition of GO, IL-rGO, and Trp-AuNPs@IL-rGO. As shown in Fig. 1g, GO and IL-rGO exhibited two main binding energies for graphitic sp^2 carbon atoms and oxygenate groups at approximately 285 eV and 530 eV, respectively. The N 1s band appeared on the IL-rGO and centered at 401.7 eV with a lower binding energy shoulder at 399.9 eV (Figs. S3a, S3b, and S3c), indicating the successful attachment of IL-NH_2 to the graphene sheets (Huang et al., 2018). Compared to GO, there was an additional component at 285.55 eV in IL-rGO, which was accompanied by dramatic decreases in epoxy groups. This new component was attributed to the combination of the C bound to nitrogen, which newly appeared after the reaction and the C–N groups from the imidazolium ring of the ionic liquid. Additionally, the Au 4f high-resolution XPS spectrum of Trp-AuNPs@IL-rGO in Fig. S3d indicated the presence of an Au 4f doublet (83.7 eV and 87.45 eV) on the Trp-AuNPs@IL-rGO. This was consistent with the Au^0 state and confirmed the presence of AuNPs on the surface of IL-rGO. Taken together, the above-described results further demonstrated the successful preparation of Trp-AuNPs@IL-rGO.

2.2. Comparison of AuNP nanocomposites reduced by five different kinds of amino acids

Natural amino acids possess abundant chelating and functional groups with specific reducibility and affinities to Au atoms, all of which make them ideal green reductants (Li et al., 2016b). Furthermore, AAs also stabilize AuNPs, as AAs with the same electric charge of the amino acids attached to the AuNPs surface repel each other and spread evenly. As shown in Fig. S4, after centrifugation, the AuNPs agglomerated and formed a black dot when the AAs is cleaned. To obtain optimal analytical performances, we compared the properties of AuNPs reduced by five typical natural amino acids with different R groups, namely Tryptophan (Trp), Lysine (Lys), Asparagine (Asn), Aspartic acid (Asp), and Valine (Val) (Fig. S5). As shown in Fig. 2, all of the amino acids rapidly produced evenly-sized AuNPs, acting both as reductants and stabilizers. However, the color of the gold solution and particle size varied significantly depending on the AA used. The Trp-AuNPs were approximately 5.186 ± 0.629 nm, while Lys-AuNPs, Asn-AuNPs, Asp-AuNPs, and Val-AuNPs gradually increased with the average particle size of 19.92 ± 0.45 nm, 20.22 ± 1.07 nm, 29.78 ± 0.61 nm, and 49.09 ± 1.44 nm in order. Interestingly, the smaller the particle size of the gold nanoparticles, the lighter the color of the solution (Fig. 2a–f). Previous studies have indicated that the more potent reductants yield smaller, spherical, and smooth nanomaterials with better catalytic properties (Briggs et al., 2015; Li et al., 2016b). Additionally, the molecular simulations showed that the amino acids preferentially attached to 4.0 nm and 2.0 nm AuNPs (Shao and Hall, 2016). Therefore, the above evidence suggested that Trp had the best reduction ability among the five AAs tested.

Fig. 3a illustrates the synthesis of GRα-BSA-AbGRα-AA-AuNPs@IL-rGO. The final product AA-AuNPs@IL-rGO shown in Fig. 1a contains abundant –NH_2 and –COOH groups on the surface of AA-AuNPs. Under the activation of EDC/NHS, the –COOH groups of AA-AuNPs are blocked by ethylenediamine, and therefore only –NH_2 groups are exposed. AA-AuNPs rich in –NH_2 groups are great candidates for biosensors, as they can act as a linker to easily immobilize the F_{ab} shoulder and F_c bottom of the antibody via the amino carboxyl interactions. Thus, the characteristics of AA-AuNPs for antibody immobilization and antigen detection were also assessed in this study. Antibody immobilization ability was tested in 96-well plates, and the results were shown in Fig. 3b. Amino acid-coated gold nanoparticles had a markedly higher ability to immobilize antibodies than the intact ones, particularly Trp-AuNPs. Differential pulse voltammetry (DPV) was conducted to compared the antigen detection abilities of AA-AuNPs@IL-rGO ($\triangle I$ was calculated to characterize antigen detection capacities). As illustrated in Fig. 3c, AA-AuNPs@IL-rGO/GCE had higher sensitivities towards GRα compared to bare AuNPs@IL-rGO/GCE, whereas Trp-AuNPs@IL-rGO/GCE exhibited the best analytical ability. This was because smaller-sized nanomaterials have a larger specific surface area, thus providing more binding sites and facilitating the antibody fixation to capture more targets (Raghav and Srivastava, 2016).

2.3. Electrochemical characterization

To explore the electroactivity of the obtained nanocomposites on the Trp-AuNPs@IL-rGO/GCE before GRα detection, cyclic voltammetry (CV) was recorded for each different modified electrode with a probe of 5.0 mM $[Fe(CN)_6]^{3-/4-}$ in a 0.1 M KCl aqueous solution at a scan rate of 100 mV s^{-1} (Fig. 4a). Compared with the bare GCE electrode (black curve), the redox peak current elevated after the modification of rGO on

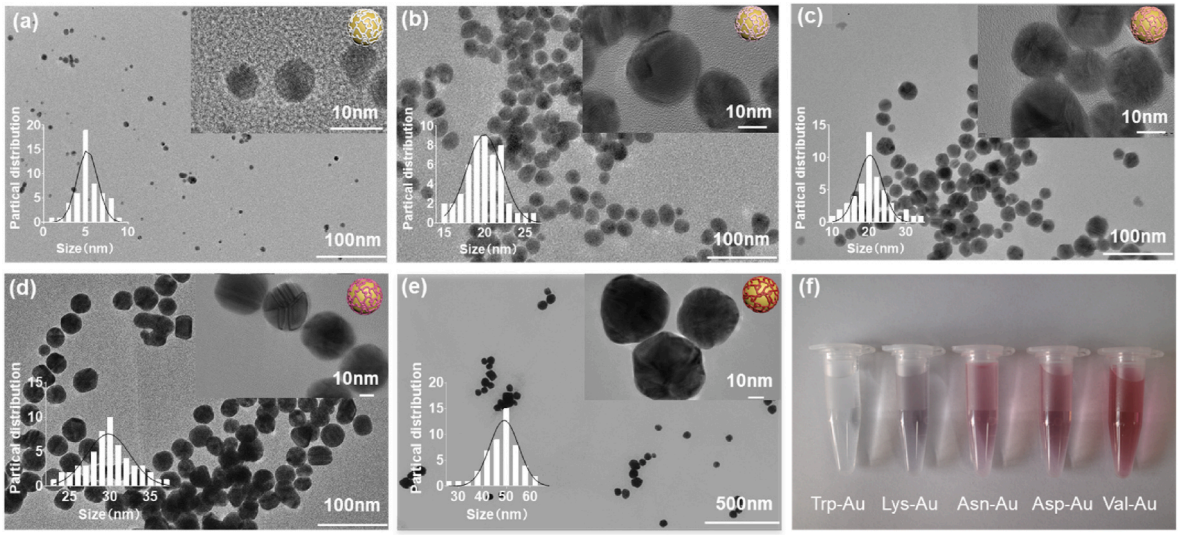

Fig. 2. Characterizations of gold nanoparticles coated with different AAs. TEM image of (a) Trp-AuNPs, (b) Lys-AuNPs, (c) Asn-AuNPs, (d) Asp-AuNPs, (e) Val-AuNPs. (f) Picture of different amino acids coated with gold nanoparticles.

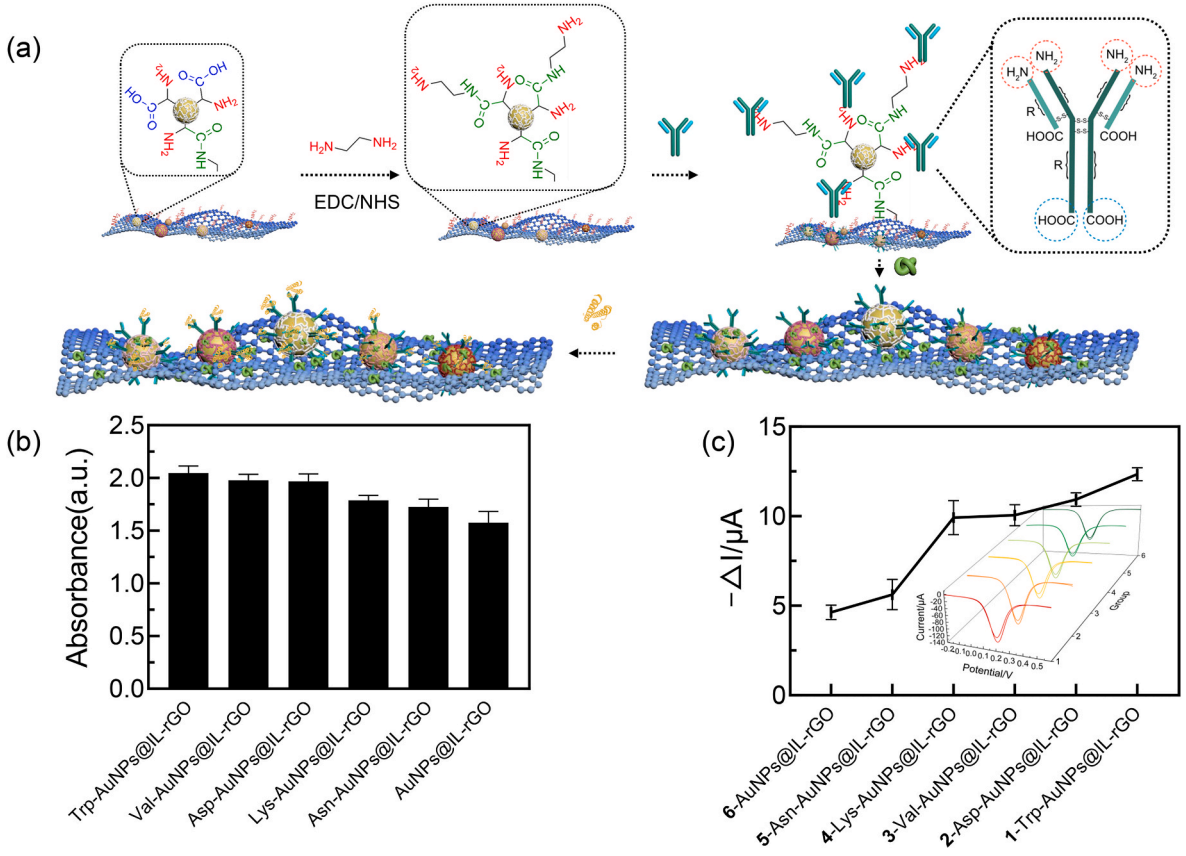

Fig. 3. Synthesis of GRα-BSA-AbGRα-AA-AuNPs@IL-rGO (a) and analysis of the properties of gold nanoparticles coated with different amino acids. (b) Immobilization capacity of the antibody in terms of the absorbance (n = 3). (c) Antibody fixation ability test. The figure inset represents the biosensing platform composed of gold reduced by different amino acids before and after GRα detection. (n = 3).

the GCE electrode (orange curve). When grafting of IL to the rGO surface (IL-rGO, blue curve), the redox peak current further increased further. In addition, a noticeable increment in the peaks was observed for AuNPs@IL-rGO/GCE (green curve), whereas Trp-AuNPs@IL-rGO (purple curve) further boosted the electron transfer on the GCE. Electroactive surface areas were quantitatively estimated according to the Randles-Sevcik equation (Lei et al., 2018; Li et al., 2021):

$$I_{pc} = 2.69 \times 10^5 n^{3/2} A_{eff} D^{1/2} v^{1/2} C_0 \quad (1)$$

where I_{pc} represents is the cathodic peak current, n is the electron transfer number, A_{eff} corresponds to the electroactive surface area (cm^2), D is the diffusion coefficient of the $[Fe(CN)_6]^{3-/4-}$ ($D = 6.70 \pm 0.02 \times 10^{-6}\ cm^2\ s^{-1}$) redox probe, v is the scan rate (0.1 $V\ s^{-1}$), and C_0 is the

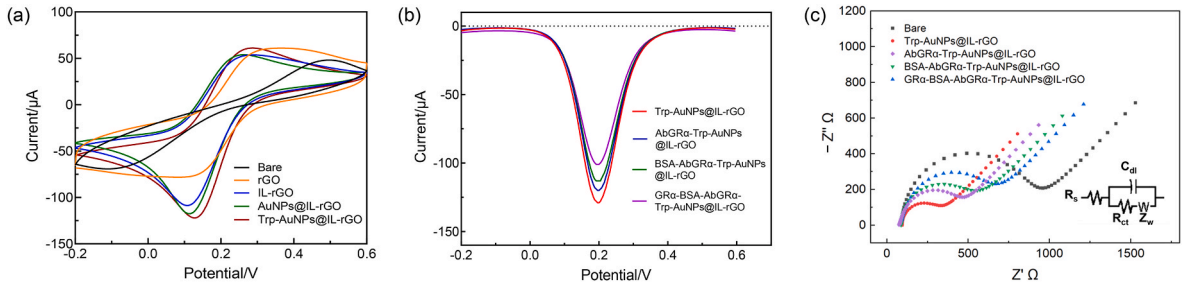

Fig. 4. Electrochemical analysis of layer-by-layer modification of GCE for the fabrication of the proposed. (a) CVs of bare, rGO, IL-rGO, AuNPs@IL-rGO and Trp-AuNPs@IL-rGO based on GCE. (b) DPV and (c) EIS results during the step-by-step construction of the biosensors.

concentration of the probe molecule ($mmol\ cm^{-3}$) (Wang et al., 2020). The calculated electroactive surface area using Eq. (1) for the Trp-AuNPs@IL-rGO/GCE modified electrode was $5.93 \times 10^{-2}\ cm^2$, which was 2.44, 1.95, 1.27, and 1.06 times higher than those of bare GCE, rGO/GCE, IL-rGO/GCE, and Au@IL-rGO/GCE, respectively. These remarkable enhancements in electrochemical signals were likely because IL-rGO modified the irreversible agglomerates of rGO on the electrode surface, thus increasing the active surface area with more arching sites for AuNPs (Li et al., 2016a). Additionally, both the good conductivity of AuNPs and the protonation and deprotonation of amino acids accelerated the transmission of electrons (Yuan et al., 2016). Therefore, the electrode functionalized with Trp-AuNPs@IL-rGO displayed extraordinary electrochemical activity towards GRα detection.

DPV and electrochemical impedance spectra (EIS) measurements were performed to evaluate step-by-step variations during the biosensor construction process. As illustrated in Fig. 4b, the layer-by-layer immobilization of GRα antibodies (AbGRα) (blue curve), BSA (green curve), and GRα (purple curve) on AuNPs@IL-rGO/GCE, resulted in a gradual decrease in the current peaks, as modified nonconductive protein molecules hampered the electron transfer. Furthermore, EIS was used to confirm the successful fabrication of the proposed biosensor. As demonstrated by the Nyquist plots shown in Fig. 4c, the charge transfer resistance (R_{ct}) of electrodes describing a resistive behavior of the different modified electrodes immersed in the $[Fe(CN)_6]^{3-/4-}$ solution indicated that they all exhibited resistive behavior (Kim et al., 2015). Compared with the bare GCE electrode (black curve), the resistance (Rct) of Trp-AuNPs@IL-rGO/GCE was markedly lower, whereas Rct gradually increased upon AbGRα, BSA, and GRα modification, demonstrating that the GRα biosensor was successfully constructed.

2.4. Optimization of experimental variables

As shown in Fig. S6, the experimental variables were further studied, as they could directly influence the performance of the GRα biosensor. Control experiments using 0.0 and 10.0 ng mL^{-1} GRα standards were performed with the biosensors prepared on the existing Trp-AuNPs@IL-rGO/GCE in various conditions to optimize their performance and GRα detection abilities (Fig. S6). Specifically, the volume of Trp-AuNPs@IL-rGO suspension (Fig. S6a), AbGRα incubation times (Fig. S6b), AbGRα concentration (Fig. S6c), and GRα incubation time (Fig. S6d) were evaluated. The optimization criteria were established according to the generated blank signal ratio (B/S). Detection was significantly improved when the electrochemical measurements were performed under the following conditions: 10 μL volume of Trp-AuNPs@IL-rGO (B/S 1.36), AbGRα incubation times of 90 min (B/S 1.09), AbGRα concentration of 75 μg mL^{-1} (B/S 1.16) and GRα incubation time of 120 min (B/S 1.09). These optimal conditions were thus chosen for GRα detection in downstream experiments.

2.5. Analytical characteristics

The analytical performance of the obtained GRα biosensor was evaluated via DPV under the optimized working conditions described in the previous section (Fig. 5). The ΔI values (i.e., the difference between the currents measured in the presence and absence of antigen) increased with higher GRα concentrations. The proposed biosensor exhibited two clear linear correlations between ΔI and the logarithm of the GRα concentrations from 0.001 to 50 ng mL^{-1} and from 50 to 500 ng mL^{-1}, with the linear regression equation $\Delta I\ (\mu A) = 1.907 \times \lg [GR\alpha] + 6.592$ ($R^2 = 0.9907$), and $\Delta I\ (\mu A) = 14.07 \times \lg [GR\alpha] - 14.63$ ($R^2 = 0.9904$), respectively. According to the 3 s_b/m criterion, where s_b was estimated as the standard deviation for 20 measurements conducted in the absence of GRα and m was the slope value of the calibration plot, the calculated limit of detection (LOD) was 0.283 pg mL^{-1}. The analytical capacity of the proposed sensor was compared with those of previously described methods (Table S1). Conventional methods such as western blot and RT-qPCR are commonly qualitative and semi-quantitative. However, our proposed sensor can accurately determine the concentration of the target, suggesting that the obtained sensor is more suitable for the study of depression.

Reproductivity, long-term stability and specificity are critical factors that must be evaluated to assess the efficiency and applicability of biosensors. Therefore, total GRα protein was determined in clinical samples (blood cells and tissue extracts) to assess the potential interference from non-target molecules, including IL-6, glucose oxidase (GOD), cholesterol esterase (ChOx), lactate dehydrogenase (LD), and ganglion esterase (GE). Measurements were conducted by testing 10 ng mL^{-1} GRα standard solutions in the absence and presence of non-target proteins at various concentrations representative of serum levels of healthy individuals. As shown in Fig. S7a, no significant B/S ratios were observed between the different experimental groups, and the non-target proteins caused little to no interference, thus demonstrating that the GRα protein could be determined in a complex system.

The stability of the BSA-AbGRα-Trp-AuNPs@IL-rGO/GCE was assessed by storing different electrodes at 4 °C in a humid chamber. The stored bioelectrodes were used as daily controls to measure 0 and 10 ng mL^{-1} GRα standard solutions. Fig. S7b showed that there were no significant differences between the B/S ratios of the prepared biosensors for at least 15 days, illustrating an acceptable stability. Moreover, the response reproducibility of different biosensors was also evaluated using five different biosensors prepared in the same manner in the same (intra-assay) or different (inter-assay) days. As shown in Fig. S7c, the assay was highly reproducible, with RSD values of 1.1% and 1.3%, respectively.

2.6. Detection of GRα in hippocampus and blood cells

To corroborate the clinical applicability of our proposed approach, the biosensor was used to detect GRα in clinical. In this study, GRα levels in both hippocampus and blood cells from different groups [control (health), model (depression) and fluoxetine (depression with fluoxetine)] were tested (Fig. 6a). Only small amounts of diluted samples (less than 3 μL) were needed for effective GRα detection. ELISA and western blot were also used to assure the consistency and reliability of the results. Firstly, the accomplishment of constructing depression model was

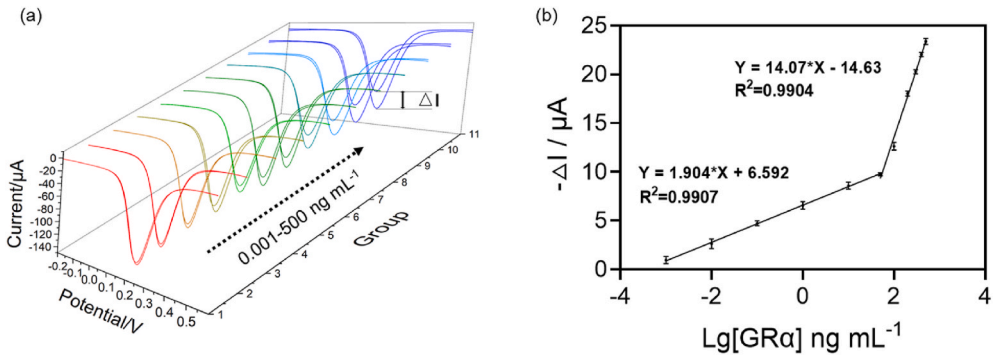

Fig. 5. Amperometric (△I) detection of GRα from 1 pg mL^{-1} to 500 ng mL^{-1} with the BSA-AbGRα-Trp-AuNPs@IL-rGO/GCE biosensor. (a) Original DPV data. (b) Standard curve.

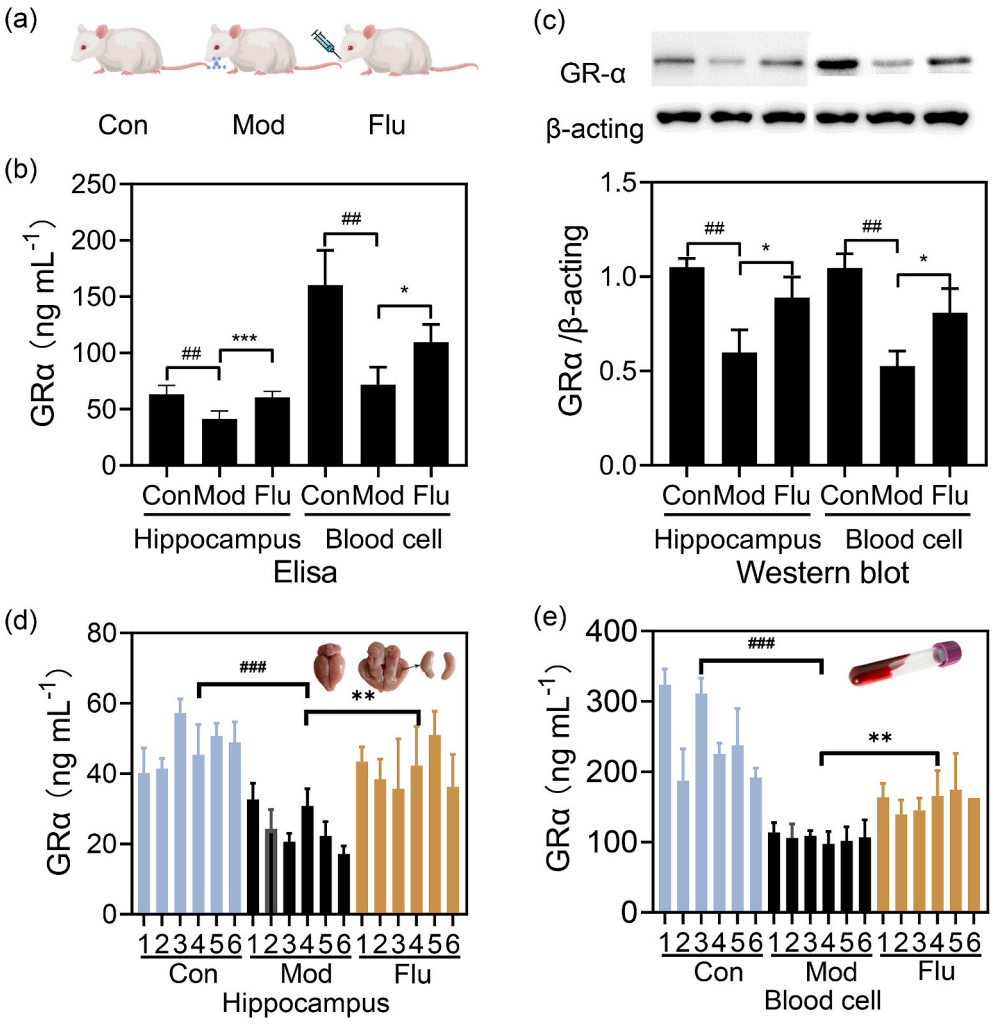

Fig. 6. Detection of GRα in hippocampus and blood cells from of the control group (Con-grey), model group (Mod-black), and fluoxetine group (Flu-Golden) with commercial kits and the proposed biosensor. (a) Schematic diagram of animal treatments (n = 6). (b) Enzyme-linked immunosorbent assay and (c) western blot. (d) Amperometric responses of GRα in the hippocampus. (e) Amperometric responses of GRα in blood cells. ##P<0.01 vs. Con; ***P<0.001, **P<0.01 and *P<0.05 vs. Mod (n = 6).

confirmed. Compared with the control group, the GRα levels in the model group were significantly lower in both the hippocampus and blood cells (Fig. 6b and c). In contrast, under fluoxetine treatment, the suppression of GRα expression was alleviated, thus demonstrating the successful establishment of the depression model.

To explore whether the obtained sensor could be applied for the detection of native GRα, the amperometric responses were tested in samples collected from different groups (Fig. 6d and e). The biosensor responses in the healthy group were significantly higher than in the depression group, whereas a marked increment could be observed in the fluoxetine group. The results were consistent with the results of the western bolt and ELISA methods, as well as with previous reports. The specific data obtained by the biosensor is shown in Table S2. In addition, the sample recovery of the proposed GRα sensor was also investigated (Table S3). An acceptable recovery rate was obtained, which strongly endorsed that the biosensor offers a satisfactory platform for depression study in the near future.

3. Conclusions

In this work, we developed a novel electrochemical biosensing platform for the accurate and sensitive detection of depression using the GRα protein as a biomarker for the first time. AA-coated AuNPs and IL-rGO were employed to enhance the simplicity and sensitivity of the proposed biosensor, resulting in ultrasensitive, convenient, and cost-effective GRα analysis. Due to their unique features, AAs not only serve as reducing agents and stabilizers, but also as bridging agents when constructing the sensing surface. After screening the performances of AA-AuNPs@IL-rGO using five typical amino acids, Trp-AuNPs@IL-rGO exhibited optimal properties and was thus selected as the final matrix to load the GRα antibodies. The sensor based on BSA-AbGRα-Trp-AuNPs@IL-rGO/GCE exhibited an extraordinary analytical performance, with a detection range from 0.001 ng mL^{-1} to 500 ng mL^{-1} and a LOD value of 0.283 pg mL^{-1}. Additionally, the GRα levels in both the hippocampus and blood cells could be tested with the proposed sensor and exhibited a delightful correlation with the ELISA and western bolt results. The obtained sensor could precisely discriminate GRα differences in healthy and depressive rats without large amounts of sample or incubation with secondary antibodies. Further, GRα differences after fluoxetine treatment could also be accurately identified. This novel and simple methodology will be a significant step forward in depression diagnosis and related drug discovery, where a lack of objective and straightforward approach becomes a great "stumbling block" for its in-depth study.

Experimental section

Materials and specific experimental procedures are provided in the supporting information.

All animals received care in compliance with the guidelines outlined in the Guide for the Care and Use of Laboratory Animals, and rats experiment protocols were approved by the animal ethical and welfare committee with the approval No. IRM-DWLL-2020111.

Credit author statement

Shengnan Yang: Conceptualization, Methodology, Investigation, Formal analysis, Writing – original draft, Visualization, Writing – review & editing; **Wei Feng:** Investigation, Formal analysis. **Lan Xue:** Investigation, Validation. **Mengai Yin:** Investigation. **Binshuai Li:** Writing – review & editing. **Lina Lu:** Writing – review & editing. **Fuju Dai:** Writing – review & editing. **Jun Jiao:** Writing – review & editing, Writing – original draft. **Qiang Chen:** Supervision, Project administration, Funding acquisition, Writing – review & editing.

Declaration of competing interest

The authors declare that they have no known competing financial interests or personal relationships that could have appeared to influence the work reported in this paper.

Acknowledgments

This work is supported by the National Natural Science Foundation of China, China (Grant Nos. 81871451). Also supports from Tianjin Science and Technology Committee, China (Grant Nos. S20YBL760).

Appendix A. Supplementary data

Supplementary data to this article can be found online at https://doi.org/10.1016/j.bios.2022.113972.

References

Abbasi, H., Puusepp-Benazzouz, H., 2020. JAMA Pediatr. 174, 908-908.
Azadbakht, A., Abbasi, A.R., Derikvand, Z., Karimi, Z., Roushani, M., 2016. Nano-Micro Lett. 9, 4.
Briggs, B.D., Li, Y., Swihart, M.T., Knecht, M.R., 2015. ACS Appl. Mater. Interfaces 7, 8843–8851.
Cai, L., Yu, G., 2021. Adv. Mater. 33, 2004974.
Canet, G., Chevallier, N., Zussy, C., Desrumaux, C., Givalois, L., 2018. Front. Neurosci. 12, 739.
D'Alessio, L., Mesarosova, L., Anink, J.J., Kochen, S., Solís, P., Oddo, S., Konopka, H., Iyer, A.M., Mühlebner, A., Lucassen, P.J., Aronica, E., van Vliet, E.A., 2020. Epilepsia 61, 1595–1605.
Danczak, A., 2017. Br. Med. J. 359 j4736-j4736.
Dou, X.-Q., Feng, C.-L., 2017. Adv. Mater. 29, 1604062.
Feng, L., Gao, G., Zhang, C., Ma, J., Cui, D., 2014. J. Exp. Nanosci. 9, 452–462.
Ferenchick, E.K., Ramanuj, P., Pincus, H.A., 2019. Br. Med. J. 365, 1794.
Georgakilas, V., Tiwari, J.N., Kemp, K.C., Perman, J.A., Bourlinos, A.B., Kim, K.S., Zboril, R., 2016. Chem. Rev. 116, 5464–5519.
Gilbert, D., 2017. Br. Med. J. 358, j4207.
Gormley, G.J., Lowy, M.T., Reder, A.T., Hospelhorn, V.D., Antel, J.P., Meltzer, H.Y., 1985. AM. J. Psychiat 142, 1278–1284.
Gururajan, A., Reif, A., Cryan, J.F., Slattery, D.A., 2019. Nat. Rev. Neurosci. 20, 686–701.
Huang, Y., Wei, Q., Wang, Y., Dai, L., 2018. Carbon 136, 150–159.
Huckins, L.M., 2017. Lancet Psychiatr. 4, 654–656.
Keller, J., Gomez, R., Williams, G., Lembke, A., Lazzeroni, L., Murphy, G.M., Schatzberg, A.F., 2017. Mol. Psychiatr. 22, 527–536.
Kim, D., Han, S.A., Kim, J.H., Lee, J.-H., Kim, S.-W., Lee, S.-W., 2020. Adv. Mater. 32, 1906989.
Kim, K.S., Jang, J.-r., Choe, W.-S., Yoo, P.J., 2015. Biosens. Bioelectron. 71, 214–221.
Knable, M.B., Barci, B.M., Webster, M.J., Meador-Woodruff, J., Torrey, E.F., 2004. Mol. Psychiatr. 9, 609–620.
Lee, H.-E., Ahn, H.-Y., Mun, J., Lee, Y.Y., Kim, M., Cho, N.H., Chang, K., Kim, W.S., Rho, J., Nam, K.T., 2018. Nature 556, 360–365.
Lei, M., Fu, C., Cheng, X., Fu, B., Wu, N., Zhang, Q., Fu, A., Cheng, J., Gao, J., Zhao, Z., 2017. Adv. Funct. Mater. 27, 1700978.
Lei, T., Chen, W., Lv, W., Huang, J., Zhu, J., Chu, J., Yan, C., Wu, C., Yan, Y., He, W., Xiong, J., Li, Y., Yan, C., Goodenough, J.B., Duan, X., 2018. Joule 2, 2091–2104.
Li, D., Dai, L., Ren, X., Ji, F., Sun, Q., Zhang, Y., Ci, L., 2021. Energy Environ. Sci. 14, 424–436.
Li, L., Zhang, Y., Shang, T., Guo, H., Liu, X., Lu, X., 2016a. J. Electroanal. Chem. 781, 218–222.
Li, X., Li, N., Zhao, L., 2016b. Sci. Bull. 61, 1732–1738.
Mackin, R.S., Insel, P.S., Landau, S., Bickford, D., Morin, R., Rhodes, E., Tosun, D., Rosen, H.J., Butters, M., Aisen, P., Raman, R., Saykin, A., Toga, A., Jack Jr., C., Koeppe, R., Weiner, M.W., Nelson, C., Alzheimers Dis Neuroimaging, I., Project, A. D., 2021. Biol. Psychiatr. 89, 757–765.
Malhi, G.S., Mann, J.J., 2018. Lancet 392, 2299–2312.
Matsubara, T., Funato, H., Kobayashi, A., Nobumoto, M., Watanabe, Y., 2006. Biol. Psychiatr. 59, 689–695.
Matsumoto, M., Saito, Y., Park, C., Fukushima, T., Aida, T., 2015. Nat. Chem. 7, 730–736.
Milaneschi, Y., Simmons, W.K., van Rossum, E.F.C., Penninx, B.W.J.H., 2019. Mol. Psychiatr. 24, 18–33.
Okada, Y., Okada, M., 2020. Mol. Biol. Rep. 47, 1021–1032.
Pariante, C.M., Lightman, S.L., 2008. Trends Neurosci. 31, 464–468.
Perlman, W.R., Webster, M.J., Kleinman, J.E., Weickert, C.S., 2004. Biol. Psychiatr. 56, 844–852.
Preiss, L.C., Werber, L., Fischer, V., Hanif, S., Landfester, K., Mastai, Y., Muñoz-Espí, R., 2015. Adv. Mater. 27, 2728–2732.
Raghav, R., Srivastava, S., 2016. Biosens. Bioelectron. 78, 396–403.
Rahman, M., Cui, D., Zhou, S., Zhang, A., Chen, D., 2020. Anal. Methods 12, 440–447.
Rotenstein, L.S., Ramos, M.A., Torre, M., Segal, J.B., Peluso, M.J., Guille, C., Sen, S., Mata, D.A., 2016. JAMA 316, 2214–2236.
Shao, Q., Hall, C.K., 2016. Langmuir 32, 7888–7896.
Song, M., Pang, S.-Y., Guo, F., Wong, M.-C., Hao, J., 2020. Adv. Mater. 7, 2001546.
Sousa, V.C., Mantas, I., Stroth, N., Hager, T., Pereira, M., Jiang, H., Jabre, S., Paslawski, W., Stiedl, O., Svenningsson, P., 2020. Mol. Psychiatr. 188, 4025.
Stoller, M.D., Park, S., Zhu, Y., An, J., Ruoff, R.S., 2008. Nano Lett. 8, 3498–3502.
Sun, X., Deng, X., Cai, W., Li, W., Shen, Z., Jiang, T., Huang, J., 2018. Life Sci. 195, 33–43.
Vigo, D., Thornicroft, G., Atun, R., 2016. Lancet Psychiatr. 3, 171–178.
Wang, Z., Yang, S., Wang, Y., Feng, W., Li, B., Jiao, J., Han, B., Chen, Q., 2020. Anal. Chim. Acta 1140, 145–152.
Xing, P., Chen, H., Xiang, H., Zhao, Y., 2017. Adv. Mater. 30, 1705633.
Xu, D., Zhang, L., Wang, H., Bian, Z., 2019. Chem. Eng. J. 358, 1371–1382.
Yu, C., Fang, H., Liu, Z., Hu, H., Meng, X., Qiu, J., 2016. Nano Energy 25, 184–192.
Yuan, F., Wang, Q., Yang, P., Cong, W., 2016. Separ. Purif. Technol. 168, 257–264.
Zhou, B., Zhu, Z., Ransom, B.R., Tong, X., 2021. Mol. Psychiatr. 26, 103–117.